THE EUROPEAN
PHYSICAL JOURNAL C

Dynamical approach to MPI four-jet production in Pythia

B. Blok[1,a], **P. Gunnellini**[2,b]

[1] Department of Physics, Technion-Israel Institute of Technology, Haifa, Israel
[2] Deutsches Elektronen-Synchrotron (DESY), Notkestraße 85, 22761 Hamburg, Germany

Abstract We modify the treatment of multiple parton interactions (MPI) in PYTHIA by including the $1 \otimes 2$ mechanism and treating the $2 \otimes 2$ mechanism in a model-independent way. The $2 \otimes 2$ mechanism is calculated within the mean field approximation, and its parameters are expressed through generalized parton distributions extracted from HERA data. The parameters related to the transverse parton distribution inside the proton are thus independent of the performed fit. The $1 \otimes 2$ mechanism is included along the lines of the recently developed formalism in perturbative QCD. A unified description of MPI at moderate and hard transverse momenta is obtained within a consistent framework, in good agreement with experimental data measured at 7 TeV. Predictions are also shown for the considered observables at 14 TeV. The corresponding code implementing the new MPI approach is made available.

1 Introduction

It is widely realized now that hard *multiple parton interactions* (MPI) play an important role in the description of inelastic proton–proton (pp) collisions at high center-of-mass energies. Starting from the 1980s [1–5] until the last decade [6–32], extensive theoretical studies have been carried out. Attempts have been made to incorporate multiparton collisions in Monte Carlo (MC) event generators [33–37]. Multiple parton interactions can serve as a probe for *nonperturbative correlations* between partons in the nucleon wave function and are crucial for determining the structure of the underlying event (UE) at Large Hadron Collider (LHC) energies. Moreover, they constitute an important background for new physics searches at the LHC. A large number of experimental measurements have been performed at the Tevatron [38–40] and at the LHC [41–44], showing evidence for MPI

at both soft and hard scales. This latter case is usually referred to as "double parton scattering" (DPS), which involves two hard scatterings within the same hadronic collision. The cross section of such an event is generally expressed in terms of the σ_{eff}. In the mean field approximation σ_{eff} [1–27,32], is the effective area which measures the transverse distribution of partons inside the colliding hadrons and their overlap in a collision.

Recently, a new approach based on perturbative quantum chromodynamics (pQCD) has been developed [22–25] for describing the MPI and its main ingredients are:

- The MPI cross sections are expressed through new objects, namely double generalized parton distributions (GPD$_2$);
- besides the conventional mean field parton model approach to MPI, represented by the so-called $2 \otimes 2$ mechanism (see Fig. 1 left), an additional $1 \otimes 2$ mechanism (Fig. 1 right) is included. In this mechanism, which can be described in pQCD, the parton from one of the nucleons splits at some hard scale and creates two hard partons that may participate in MPI. This mechanism leads to a significant transverse-scale dependence of MPI cross sections.
- The contribution of the $2 \otimes 2$ mechanism to GPD$_2$ is calculated in a mean field approximation with model-independent parameters.

The use of this new formalism at LHC experiments needs its implementation in MC event generators, which has not been performed yet. The purpose of the present paper is to make a step ahead toward the implementation of this formalism into MC generators. We use the standard simulation of the MPI implemented in PYTHIA [35], but with values of σ_{eff} calculated by using the QCD-based approach of [22–25], i.e. including $1 \otimes 2$ processes.

The current approach used for the description of the MPI in PYTHIA is based on [34,35]. The PYTHIA code uses parton

[a] e-mail: blok@physics.technion.ac.il
[b] e-mail: paolo.gunnellini@desy.de
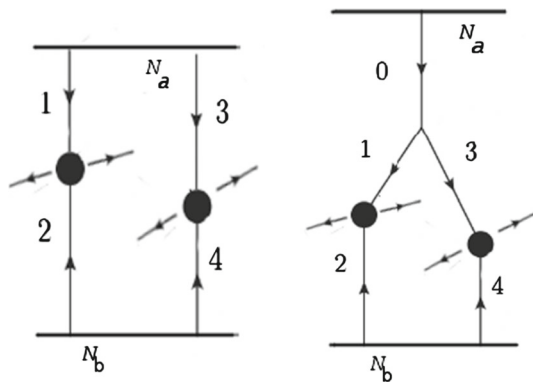
Fig. 1 Sketch of the two considered MPI mechanisms: $2 \otimes 2$ (*left*) and $1 \otimes 2$ (*right*) mechanism

distribution functions, dependent on the impact parameter of the collision. From the theoretical point of view these are just one-particle generalized parton distributions GPD$_1$ (see e.g. [45,46] for a review). The parameters set in the PYTHIA simulation relative to the transverse parton density are extracted from fits to experimental data on UE, sensitive to the contribution of the MPI. This procedure is closely related to mean field-based schemes; see e.g. [22].

Such an approach has, however, a number of difficulties, both conceptual and practical. First of all, a problem arises at the level of mean field approximation. The transverse parton distributions have been extracted from J/Ψ photoproduction measurements at the HERA collider, using QCD factorization theorems [19–21,45,46]. Hence they cannot be treated as free parameters of the model. Secondly, it has been observed that different PYTHIA parameters are obtained when data sensitive to a different region of the MPI spectrum are used for the fits. For example, it has been shown [47] that different parameters result for fits to UE or hard MPI data. This might be an indication that an additional transverse-scale dependence, which is not present in the mean field approach, is needed to describe experimental data on UE and hard MPI simultaneously. Recent improvements in the PYTHIA MPI model include a dependence of the parton transverse density on the longitudinal momentum fraction (x) [34], but this only accounts for the x values of the hardest dijet. A complete x dependence which considers soft and hard partons may be irrelevant for the UE description where the transverse scales are rather close, but it may become important for measurements sensitive to hard MPI.

The approach used in this paper combines the standard PYTHIA MPI model with the one of [22–25]. We use a single gaussian to model the matter distribution function of the protons in PYTHIA. With these settings, the value of $\sigma_{\text{eff}}^{(0)}$ would be constant and independent on the scale. In order to implement the x and the scale dependence of σ_{eff} in collisions where a hard MPI occur, these events are rescaled according to

$$\sigma_{\text{eff}} = \frac{\sigma_{\text{eff}}^{(0)}}{1 + R}, \tag{1}$$

where $\sigma_{\text{eff}}^{(0)}$ is the effective cross section in the mean field approach calculated in a model-independent way from GPD$_1$, parameterized from HERA data [19–22], and R corresponds to the correction due to the $1 \otimes 2$ mechanism [24,25]. Such an approach is equivalent to using the GPD$_1$-based transverse parton densities for parton transverse distributions.

The main result of this paper is that the approach discussed above gives a unified description of both hard MPI and UE experimental data, with good accuracy and few fit parameters. The fit parameters are related to the amount of simulated MPI and of the color string reconnection, and to the separation scale between soft- and hard-scale processes, Q_0^2, whose value is expected to lie in the range 0.5–2 GeV^2. The transverse-scale-dependent function R is calculated numerically by solving the nonlinear evolution equation [24,25]. Predictions using this approach are shown later in the paper, and they are labeled UE tune Dynamic σ_{eff}. Our analysis shows that the values of observable for UE are quite close to the results obtained in a free parton model (mean field approximation), while the inclusion of transverse-scale-dependent rescaling calculated in pQCD [24] improves the description of hard MPI.

The paper is organized as follows. In Sect. 2, basic theoretical ideas of the used approach are presented, while in Sect. 3 their MC implementation is discussed. In Sect. 4, comparisons for various predictions to observables measured at 7 TeV are shown. In Sect. 5, predictions for these observables are presented for pp collisions at 14 TeV. In Sect. 6 we compare our approach with the recently developed HERWIG-EE-5 approach, before drawing the conclusions in Sect. 7.

2 A summary of the theoretical background

The MPI four-jet cross section is characterized by the cross section σ_{eff}, which corresponds to an effective interaction area [22], and which can be written as

$$\frac{d\sigma^{\text{four-jet}}}{dt_{12}dt_{34}} = \frac{d\sigma^{\text{two-jet}}}{dt_{12}} \frac{d\sigma^{\text{two-jet}}}{dt_{34}} \times \frac{1}{\sigma_{\text{eff}}}, \tag{2}$$

where partons 1 and 2 create the first (12), and partons 3 and 4 the second (34) dijet. The pQCD calculation leads to the following expression for σ_{eff} in terms of two-particle GPD:

$$\frac{1}{\sigma_{\text{eff}}} \equiv \int \frac{d^2\vec{\Delta}}{(2\pi)^2}$$
$$\times \Big[\, _{[2]}G_2(x_1, x_3, Q_1^2, Q_2^2; \vec{\Delta})_{[2]}G_2(x_2, x_4, Q_1^2, Q_2^2; -\vec{\Delta})$$

$$+ \, _{[1]}G_2(x_1, x_3, Q_1^2, Q_2^2; \vec{\Delta})_{[2]}G(x_2, x_4, Q_1^2, Q_2^2; -\vec{\Delta})$$
$$+ \, _{[1]}G_2(x_2, x_4, Q_1^2, Q_2^2; \vec{\Delta})_{[2]}G_2(x_1, x_3, Q_1^2, Q_2^2; -\vec{\Delta}) \Big].$$
$$(3)$$

The second and third terms in Eq. (3) correspond to the $1 \otimes 2$ mechanism, when two partons are generated from the splitting of a parton at a hard scale after evolution, while the first term corresponds to the conventional case of two partons evolving from a low scale, namely the $2 \otimes 2$ mechanism. This first term can be calculated in the mean field approximation [19–22]. The momentum Δ is conjugated to the relative distance between the two participating partons. The full double GPD is a sum of two terms:

$$G_2(x_1, x_3, Q_1^2, Q_2^2, \Delta) = {}_{[1]}G_2(x_1, x_3, Q_1^2, Q_2^2, \Delta)$$
$$+ \, _{[2]}G_2(x_1, x_3, Q_1^2, Q_2^2, \Delta). \quad (4)$$

Here $_{[2]}G_2$ corresponds to the part of double GPD$_2$, when both partons are evolved from the initial nonperturbative scale, while $_{[1]}G_2$ corresponds to the case when one parton evolves up to some hard scale, where it splits into two successive hard partons, each of them in turn participating to the hard dijet event. We refer the reader to [22,23] for the detailed definitions of $_{[1]}G_2$ and $_{[2]}G_2$ and their connection to light cone wave functions of the nucleon.

For the two-parton GPD$_2$ we have

$$_{[2]}G_2(x_1, x_3, Q_1^2, Q_2^2, \Delta) = D(x_1, Q_1)D(x_3, Q_2)$$
$$\times F_{2g}(\Delta, x_1)F_{2g}(\Delta, x_3), \quad (5)$$

where $D(x, Q^2)$ is a conventional parton distribution function (PDF). The use of the mean field approximation results in

$$_{[2]}G_2(x_1, x_3, Q_1^2, Q_2^2, \Delta) = G_1(x_1, Q_1^2, \Delta)G_1(x_1, Q_1^2, \Delta)$$
$$(6)$$

and

$$G_1(x_1, Q_1^2, \Delta) = D(x_1, Q_1)F_{2g}(\Delta, x_1). \quad (7)$$

For the two gluon form factor F_{2g}, we use the exponential parametrization [21]. In fact, it leads to the same numerical results as the dipole form [19,20], but it is more convenient for calculations. This parametrization is unambiguously fixed by J/Ψ diffractive charmonium photo/electro production at HERA. The functions D are the conventional nucleon structure functions and F_{2g} can be parameterized as

$$F_{2g}(\Delta, x) = \exp(-B_g(x)\Delta^2/2), \quad (8)$$

where $B_g(x) = B_0 + 2K_Q \cdot \log(x_0/x)$, with $x_0 \sim 0.0012$, $B_0 = 4.1 \text{ GeV}^{-2}$, and $K_Q = 0.14 \text{ GeV}^{-2}$. In our implementation the central values of the parameters B_0 and K_Q

[21] have been used, which are known with an accuracy of ~ 8 %. Integrating over Δ^2, we obtain for the part of σ_{eff} corresponding to the first term in Eq. (3):

$$\frac{1}{\sigma_{\text{eff}}^{(0)}} = \frac{1}{2\pi} \frac{1}{B_g(x_1) + B_g(x_2) + B_g(x_3) + B_g(x_4)}, \quad (9)$$

where $x_{1..4}$ are the longitudinal momentum fractions of the partons participating in the $2 \otimes 2$ mechanism. This cross section corresponds to the free parton model and is model independent in the sense that its parameters are determined not from the fit of experimental LHC data, but from the fit of the single parton GPD$_1$. The maximum transversality kinematics, i.e. $4Q^2 = x_1x_2s$ for each dijet, have been considered in our approach, Q being the dijet transverse scale, and x_1, x_2 the Bjorken fractions of the jets. The second and third terms in Eq. (3) are parameterized as

$$\sigma_{\text{eff}} = \frac{\sigma_{\text{eff}}^{(0)}}{1 + R}, \quad (10)$$

where $R(Q_1^2, Q_2^2, Q_0^2)$ is calculated by solving iteratively the nonlinear evolution equation, as explained in detail in [24,25]. According to the results of [25], the dependence of R on x_i in the maximum transversality regime is very weak and can be neglected with high accuracy. The function R also depends on the physical parameter Q_0^2, which corresponds to the separation scale between soft and hard dynamics where the GPD$_2$ is assumed to factorize.

3 Monte Carlo implementation and definition of experimental observables

In this paper we carry out two types of simulations: one based on the new approach defined in the Sects. 1 and 2 and one which follows the standard PYTHIA approach, used for comparison.

Let us recall the standard PYTHIA approach which is referred as to "UE tune" hereafter. In this study we use the PYTHIA 8.185 MC event generator [33]. It simulates a $2 \rightarrow 2$ matrix element interfaced to parton shower and UE. The PYTHIA 8 event generator uses a simulation of the parton shower ordered in transverse momentum and the Lund string model [48] to implement the hadronization process. The performed study has considered as a starting point the UE simulation implemented in the PYTHIA 8 tune 4C [35]. This simulation makes use of the CTEQ6L1 [49] PDF and of a simple gaussian as a transverse matter distribution function. A fit to experimental data sensitive to the UE is performed in order to optimize the parameters related to the amount of MPI and color reconnection in the simulation. The fit operation has been carried out by using the RIVET [50] software, combined with the PROFESSOR machinery [51]. For the

Table 1 PYTHIA 8 parameters obtained after the fit to the UE observables. The value of pT0Ref is given at a reference energy of 7 TeV. The values of the reduced χ^2 and of σ_{eff} at 7 and 14 TeV are also shown in the table

PYTHIA 8 parameter	Value obtained for the UE tune
MultipleInteractions:p_{T}^0 Ref	2.659
BeamRemnants:reconnectRange	3.540
Reduced χ^2	0.647
σ_{eff} (7 TeV) (mb)	29.719
σ_{eff} (14 TeV) (mb)	32.235

tune, two different observables have been considered at a center-of-mass energy of 7 TeV measured by the ATLAS experiment [52]. They are related to the multiplicity, N_{chg}, and the sum of the transverse momentum, $p_\perp$, of the charged particles in the region transverse to the direction of the leading charged particle in each event. The performed fit has used only the data points corresponding to transverse momenta of the leading charged particle between 2.0 and 15.0 GeV. The exclusion of the very low p_T region (≤ 2 GeV) is motivated by the fact that processes at those scales are expected to be dominated by soft physics, including diffractive processes and soft nonperturbative correlations, i.e. along the lines of [23]. The upper cut off is arbitrary, since its variation starting from 5 GeV does not change the values of the observables.

The result of the fit consists of a new set of UE parameters implemented in the "UE tune" hereafter. The values of the PYTHIA 8 parameters obtained for the "UE tune" after the fit are shown in Table 1.

The first parameter listed in the table refers to the value of transverse momentum, p_T^0, defined at $\sqrt{s} = 7$ TeV, used for the regularization of the cross section in the infrared limit, according to the formula $1/p_T^4 \rightarrow 1/(p_T^2 + p_T^{0\,2})^2$. The second parameter is the probability of color reconnection among parton strings. The value of σ_{eff} is found to be around 29.7 mb at 7 TeV; this value is significantly smaller than the one obtained by tuning the correlation observables of the four-jet scenario [44], which is around 19–21 mb. Note that the value of 29.7 mb is quite close to the one determined in mean field approach [22,25].

After fitting the UE observables for the "UE tune" determination, the considered predictions are also tested against measurements sensitive to the hard spectrum of the MPI. Measurements of such a type have been conducted by studying the correlations between outgoing objects in a proton–proton collision, for instance in four-jet final states measured at 7 TeV by CMS [44]. In this scenario, two dijets have been selected at different transverse momentum; two jets are required to have p_T larger than 50 GeV and they are classified as a "hard jet pair", while the so-called "soft jet pair" is composed by the two other jets selected with p_T greater than 20

GeV. Two correlation observables that are sensitive to DPS, ΔS and $\Delta_{\text{soft}}^{\text{rel}} p_T$, have been considered. They are, respectively, the azimuthal angle between the two dijet planes and the p_T balance between the soft jets and are defined as follows:

$$\Delta S = \arccos\left(\frac{\vec{p}_T(\text{pair}_1) \cdot \vec{p}_T(\text{pair}_2)}{|\vec{p}_T(\text{pair}_1)| \times |\vec{p}_T(\text{pair}_2)|}\right), \quad (11)$$

$$\Delta^{\text{rel}} p_T = \frac{|\vec{p}_T^{\text{jet}_1} + \vec{p}_T^{\text{jet}_2}|}{|\vec{p}_T^{\text{jet}_1}| + |\vec{p}_T^{\text{jet}_2}|}, \quad (12)$$

where pair_1 (pair_2) is the hard (soft) jet pair and jet_1 (jet_2) is the leading (subleading) soft jet.

Let us now move to the new approach, based on the dynamical pQCD-based formalism, described in Sects. 1 and 2. The x and scale dependence of σ_{eff} has been implemented by reweighting on an event-by-event basis the MC simulation in presence of a hard and moderate MPI. The x dependence is given by Eq. (9), where $x_{1,2}$ are taken as the longitudinal momentum fractions of the partons participating in the hardest scattering, while $x_{3,4}$ refer to the longitudinal momentum fractions of the partons participating in the hardest MPI. The scale dependence is expressed by Eq. (10), where R takes for Q_1 and Q_2 the scales of, respectively, the hard scattering and of the hardest MPI. Different values of Q_0^2 have been considered in the range between 0.5 and 2 GeV^2.

We considered both the case of moderate MPI (i.e. MPI at scales of several GeV), relevant for UE, and the case of hard MPI.

For UE we treat separately the events where there is only one hard scattering, which are not rescaled, and the events with additional hard MPI. For the latter events two approaches were checked. First, we rescaled these events according to Eqs. (9) and (10), taking as Q_1 and Q_2 for the R function the scales of the two hardest scatterings. As shown in Sect. IV, the influence of this rescaling is very small (less than 5 %), with respect to the standard PYTHIA "UE tune". This may be connected both with the small values of R obtained for UE, and with the fact that the ladder splitting is roughly taken into account for such scales by the large value of the parameter $p_T^0 \sim 2$ GeV.

Subsequently, the second approach tried was to rescale only MPI events starting from the scale of order 4–5 GeV. When we rescale only the MPI starting from this (or a higher) scale, UE observables are not affected at all. At the same time, with this approach we avoid possible double counting effects, since at these scales the regularization formula in PYTHIA represents an ansatz for higher twist effects, including MPI. Thus, while using PYTHIA, we can neglect rescaling of MPI in UE, fitting p_T^0 instead. With the current accuracy, any of these two approaches can be used, leading to identical numerical results. This is in agreement with the approach documented in [25], where it was argued that at scales relative to UE the

values of σ_{eff} are close to the ones calculated in the mean field approximation.

We consider now the case of hard MPI, specifically DPS. Two different processes may produce four jets in the final states. The first one is the so-called single parton scattering (SPS) where the four jets are emitted through the same chain while the second one is DPS where the two hard interactions produce one dijet each. A different event topology is expected from these processes: if the four jets are produced through SPS, a high correlation between the objects of the final state is present and this is reflected in their relative configuration in the transverse plane. The direction of the hard jets, for example, is randomized by the emission of the additional two jets within the same chain and their initial p_{T} balance is ruined. Instead, jet pairs coming from DPS events, namely from two independent scatterings, tend to be uncorrelated and their initial back-to-back configuration is less subject to smearing effects coming from additional hard radiation: the jet pairs are expected to exhibit a more balanced configuration in p_{T} and azimuthal angle. In particular, as shown in [44], DPS events add a relevant contribution at low values of ΔS and $\Delta_{\text{soft}}^{\text{rel}} p_{\text{T}}$. Here we consider the experimentally relevant example, when the two dijet scales are 50 and 20 GeV.

Similarly to before, the x and scale dependence of σ_{eff} have been implemented by reweighting on an event-by-event basis the MC simulation, as explained above.

In the case that only MPI with p_{T} scales smaller than 15 GeV are present in the collision, no x and scale dependence is applied to the σ_{eff} value of the corresponding event. The choice of 15 GeV is motivated by the fact that we need to treat differently the two contributing processes, SPS and DPS. Events where the two dijets are produced through SPS accompanied by moderate MPI should not be reweighted [12,18,22–24]. In the case a hard MPI occurs in the collision, dynamical σ_{eff} values are used. In this way, we assume that all collisions with a MPI scale greater than 15 GeV produce the second hard dijet $p_{\text{T}} > 20$ GeV pair selected in the considered four-jet scenario, while MPI at lower scales are below threshold for producing jets with $p_{\text{T}} > 20$ GeV. This approach is generally followed by standard experimental measurements for σ_{eff} determination, as the ones documented in [41,42]. For our studies, lowering the 15 GeV cut off by 5–10 GeV shows variations of the predictions of DPS-sensitive observables of less than 2 %. This is a clear indication of the consistency of our approach.

Various simulation settings have been considered for comparison:

- "UE tune": predictions obtained with the parameters listed in Table 1 and without applying any reweighting of the simulation; this tune uses a constant value of σ_{eff}, following the standard PYTHIA approach;

- "UE tune Q^2-dep": predictions obtained with the UE parameters listed in Table 1 and by applying the scale dependence of σ_{eff} with $Q_0^2 = 1$ GeV^2;
- "UE tune x-dep": predictions obtained with the UE parameters listed in Table 1 and by applying the x dependence of σ_{eff};
- "UE tune Dynamic σ_{eff}": predictions obtained with the UE parameters listed in Table 1 and by applying both the x and the scale dependence with $Q_0^2 = 1$ GeV^2.

For the considered "UE tune Dynamic σ_{eff}", predictions using Q_0^2 values equal to 0.5, 1 and 2 GeV^2 have also been tested and compared.

A full MC implementation of the presented approach may be different from the one used in this paper, which relies on reweighted events simulated by PYTHIA. There are at least three reasons for it:

- By using the PYTHIA event generator, all ladders are assumed to evolve independently from the low transverse scale, the initial-state radiation (ISR) being regularized by primordial gluon distribution with a transverse scale equal to p_{T}^0. No parton ladder splittings are included in this approach.
- In PYTHIA, the geometric picture of the collisions in the impact parameter space corresponds to the $2 \otimes 2$ mechanism, while for $1 \otimes 2$ mechanism the geometrical picture would be different.
- For multi MPI events, namely for events with several MPI within the same collision, we neglect the change of relative weight of the $1 \otimes 2$ and $2 \otimes 2$ mechanisms.

In this paper, these effects are neglected. First, the good agreement with experimental data shows that the high regularization scale p_{T}^0 may be a good alternative parametrization of the ladder splittings and of the corresponding changes in ISR at the UE transverse scales. In other words, for UE the high p_{T}^0, which regularizes the charged particle multiplicity, also approximately fits the change of multiplicity due to ladder splitting. The PYTHIA regularization formula in this case can be viewed as an ansatz for twist expansion, which may include part of the MPI. Note that the ladder splitting scale is much smaller than the scales of hard dijets created by partons that evolve after the splitting [25,26]. So the effective ladder splitting is partly taken into account for UE by a high p_{T}^0 value. This is the reason why the UE observables change only slightly in the new approach. On the other hand for hard MPI, when the hard splitting scale is much larger than p_{T}^0, the inaccuracy in accounting for ISR at small p_{T} can be safely neglected.

Second, the direct calculation along the lines of [10] shows that neglecting the change of geometrical picture and of the relative weight between mean field and $1 \otimes 2$ mechanisms,

when more than two separate dijet events are present, does not lead to numerical changes.

We conclude that using events simulated with PYTHIA and reweighted with x- and scale-dependent values of $\sigma_{\rm eff}$ is a good approximation. In this way, we investigate the influence of changes of $\sigma_{\rm eff}$ on MC observables sensitive to UE and DPS.

4 Results for 7 TeV

In this section, comparisons between UE- and DPS-sensitive measurements at 7 TeV and various predictions are shown. Figure 2 shows comparisons to ATLAS data [52] on charged particle multiplicity and the $p_{\rm T}$ sum in the transverse region as a function of the leading charged particle $p_{\rm T}$. Note that these are the observables which have been used in the fitting procedure for the determination of the "UE tune". The measurement is well reproduced by all considered predictions with discrepancies of only up to 10 % in the high-$p_{\rm T}$ region ($p_{\rm T} > 10$ GeV). The intermediate $p_{\rm T}$ region ($2 < p_{\rm T} < 10$ GeV) is very well reproduced, while all predictions underestimate the first bins at $p_{\rm T} > 2$ GeV. This effect might be due to a not optimal simulation of diffraction in PYTHIA 8. However, no relevant differences are observed for the different $\sigma_{\rm eff}$ models.

In Fig. 3, predictions obtained with different values of the scale Q_0^2 are shown. All predictions are able to reproduce the measurement at the same good level. From this study,

one may conclude that the UE data are not sensitive to the different settings of dynamical dependence applied to $\sigma_{\rm eff}$.
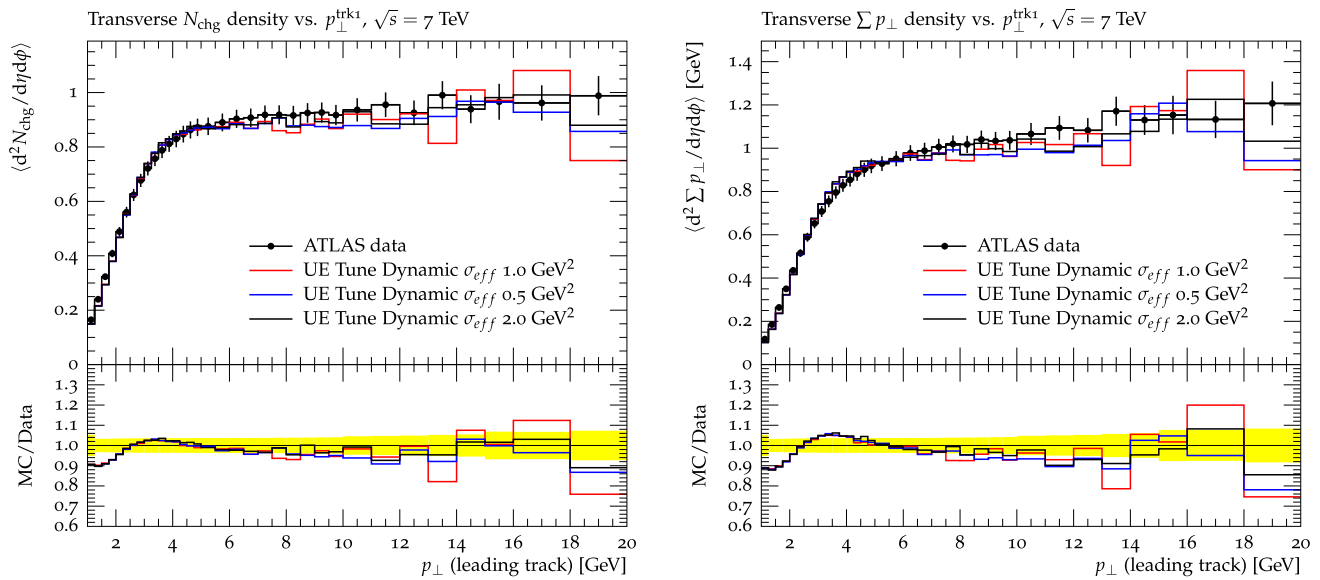
Figure 4 shows predictions with the various $\sigma_{\rm eff}$ settings considered previously, compared to the normalized cross section distributions as a function of the correlation observables, ΔS and $\Delta_{\rm soft}^{\rm rel} p_{\rm T}$, measured in four-jet scenarios [44]. For these variables, the considered models show relevant differences. The static $\sigma_{\rm eff}$ dependence ("UE tune") is not able to properly describe the distribution as a function of ΔS; in particular, the region at low values ($\Delta S < 2.5$), where a DPS contribution is expected, is underestimated by about 10–18 %. By introducing the x dependence for $\sigma_{\rm eff}$ ("UE tune x-dep"), the agreement at low values of ΔS does not significantly improve. When the scale dependence of $\sigma_{\rm eff}$ is introduced ("UE tune Q^2-dep"), the description of the normalized cross section as a function of ΔS gets better with differences not larger than 10 %. The best agreement with the measurement is obtained for predictions where both the x and the Q^2 dependence ("UE tune Dynamic $\sigma_{\rm eff}$") is included. The normalized cross section as a function of $\Delta_{\rm soft}^{\rm rel} p_{\rm T}$ is very well reproduced by all considered predictions. However, it has already been observed in [44] that $\Delta_{\rm soft}^{\rm rel} p_{\rm T}$ is less sensitive to a DPS contribution than ΔS, which uses information from both jet pairs.

In Fig. 5, predictions obtained with three different values of Q_0^2 (0.5, 1.0, and 2.0 GeV^2) are compared to the normalized cross section distributions as a function of ΔS and $\Delta_{\rm soft}^{\rm rel} p_{\rm T}$. A considerable level of agreement for the different settings is obtained. Predictions obtained with $Q_0^2 =$
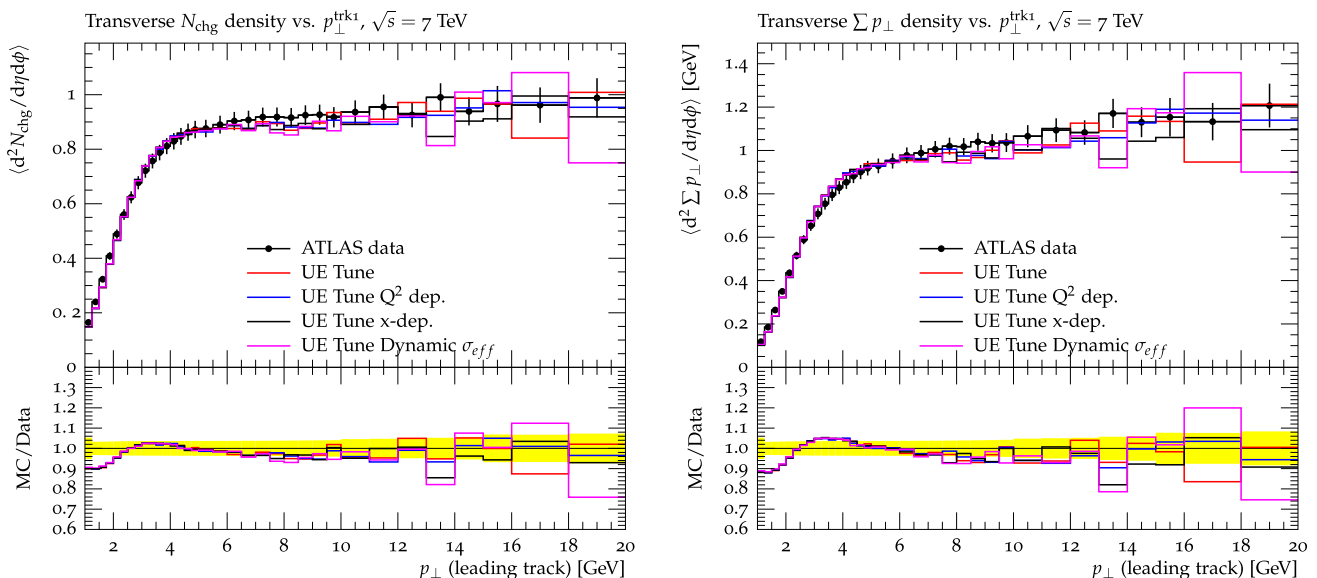

Fig. 2 Charged particle density (*left*) and $p_{\rm T}$ sum density (*right*) as a function of the leading charged particle in the transverse regions, measured by the ATLAS experiment at 7 TeV [52]. The data are compared to various predictions: the UE tune with constant $\sigma_{\rm eff}$ value (*red curve*), the UE tune with $\sigma_{\rm eff}$ x dependence applied (*blue curve*), the UE tune

with $\sigma_{\rm eff}$ scale dependence with $Q_0^2 = 1.0$ GeV^2 applied (*black curve*), and the UE tune with both $\sigma_{\rm eff}$ x and scale dependence with $Q_0^2 = 1.0$ GeV^2 applied (*pink curve*). The *lower panel* shows the ratio between the various prediction and the experimental points

Fig. 3 Charged particle density (*left*) and p_T sum density (*right*) as a function of the leading charged particle in the transverse regions, measured by the ATLAS experiment at 7 TeV [52]. The data are compared to various predictions obtained with the "UE tune" where both the x and the scale dependence have been applied for σ_{eff} with Q_0^2 equal to 1.0 (*red curve*), 0.5 (*blue curve*), and 2.0 (*black curve*) GeV^2. The *lower panel* shows the ratio between the various prediction and the experimental points
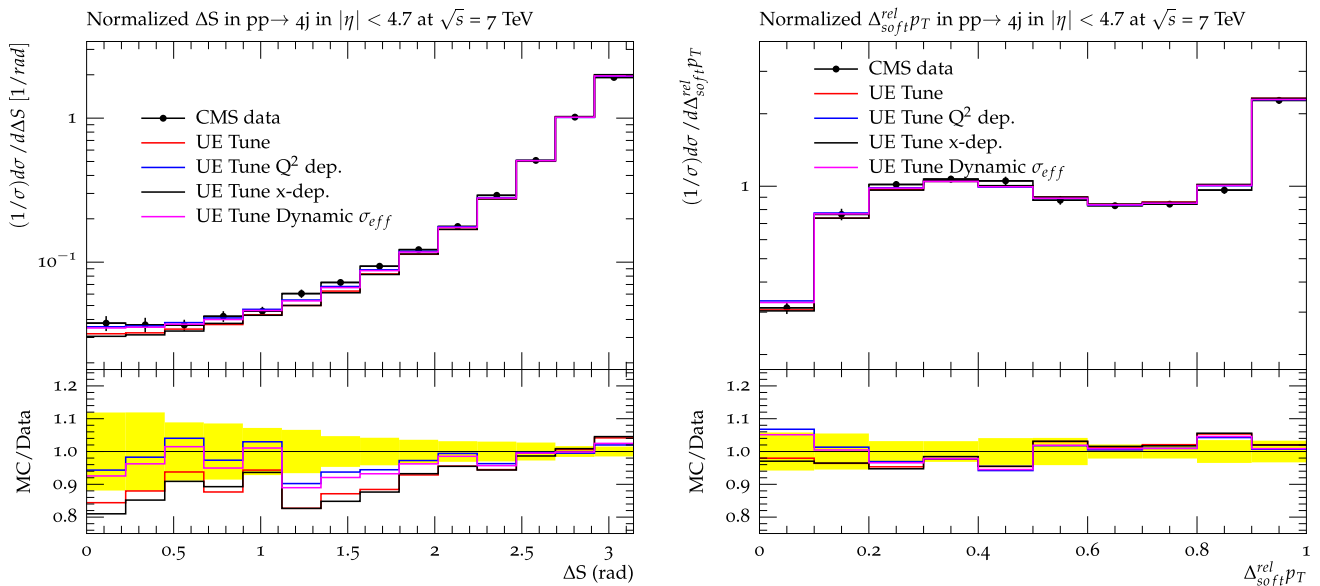
Fig. 4 Normalized cross section distributions as a function of the correlation observables ΔS (*left*) and $\Delta_{\text{soft}}^{\text{rel}} p_T$ (*right*) measured in a four-jet scenario by the CMS experiment at 7 TeV [44]. The data are compared to various predictions: the new UE tune (*red curve*), the new UE tune with the x dependence applied (*blue curve*), the new UE tune with only the scale dependence with $Q_0^2 = 1.0$ GeV^2 applied (*black curve*), and the new UE tune with both x and scale dependence with $Q_0^2 = 1.0$ GeV^2 applied (*pink curve*). The *lower panel* shows the ratio between the various prediction and the experimental points

0.5 GeV^2 are in good agreement with the ΔS measurement but overestimate the first bin of $\Delta_{\text{soft}}^{\text{rel}} p_T$. For $Q_0^2 = 1$ and 2 GeV^2 the agreement tends to improve for $\Delta_{\text{soft}}^{\text{rel}} p_T$ but is worse for ΔS. However, the measurement of the four-jet correlation observables is not able to discriminate the best choice for the value of Q_0^2.

In order to isolate the DPS contribution from the background produced by $2 \rightarrow 4$ processes, a dedicated event simulation has been performed with PYTHIA 8. Events with two hard scatterings within the same pp collision are simulated: the first hard scattering is generated with an exchanged transverse momentum between the outgoing partons, $\hat{p}_T$, larger
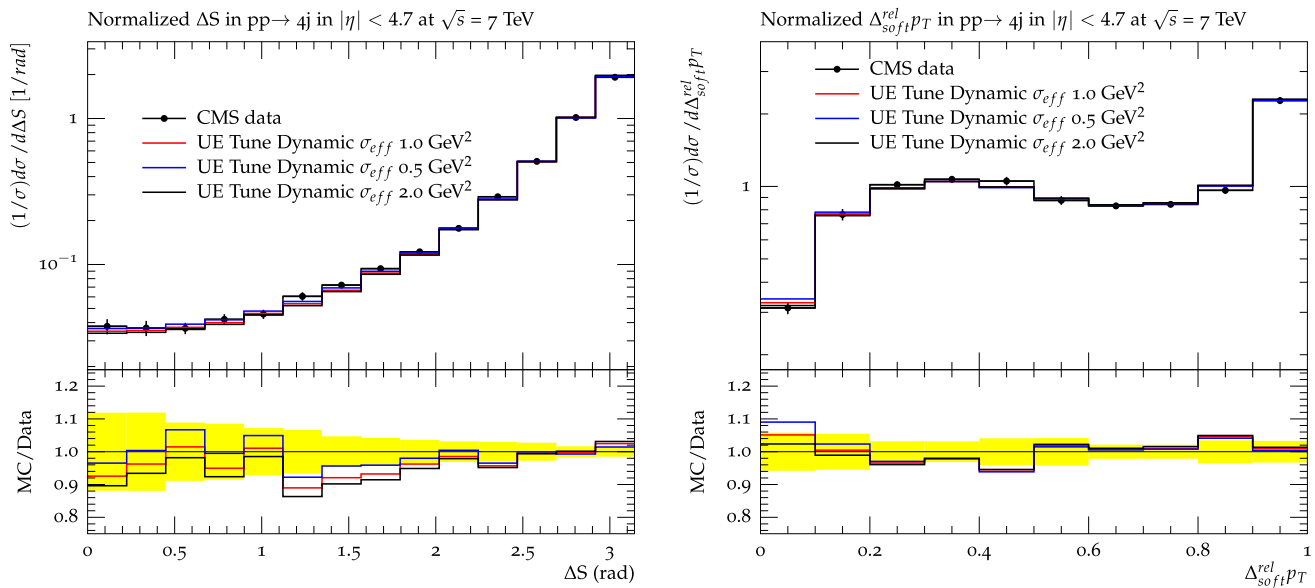
Fig. 5 Normalized cross section distributions as a function of the correlation observables ΔS (*left*) and $\Delta_{soft}^{rel} p_T$ (*right*) measured in a four-jet scenario by the CMS experiment at 7 TeV [44]. The data are compared to various predictions obtained with the new UE tune where both x and scale dependence have been applied with Q_0^2 equal to 1.0 (*red curve*), 0.5 (*blue curve*), and 2.0 (*black curve*) GeV^2. The *lower panel* shows the ratio between the various prediction and the experimental points
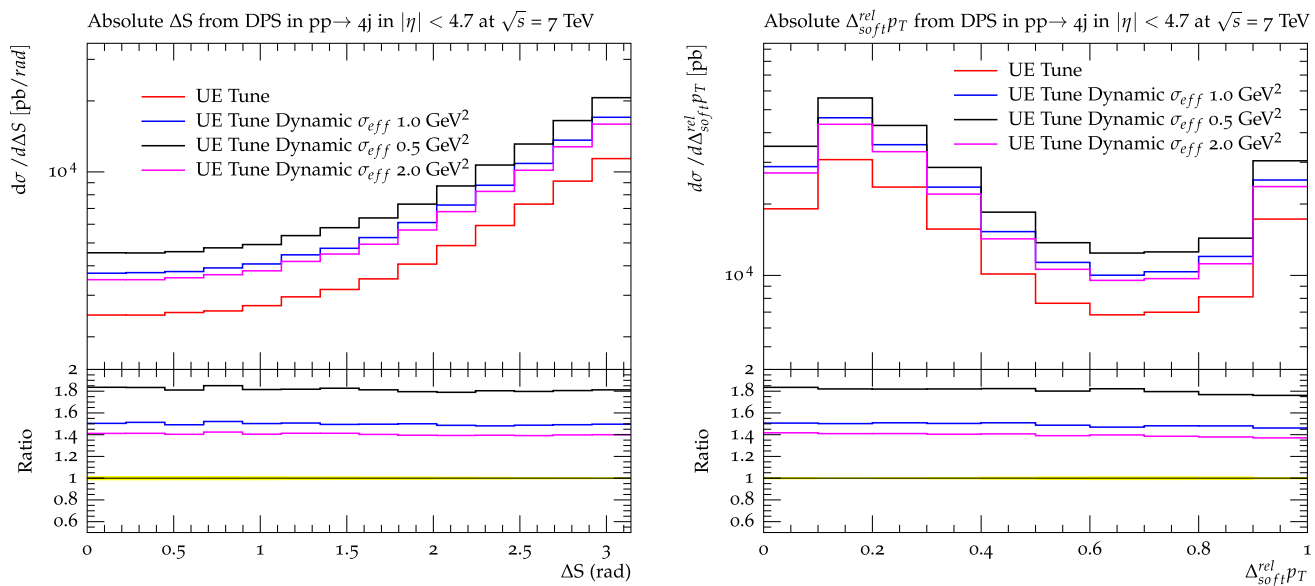
Fig. 6 Absolute cross section distributions as a function of the correlation observables ΔS (*left*) and $\Delta_{soft}^{rel} p_T$ (*right*), produced via double parton scattering in a four-jet scenario at 7 TeV. Various predictions are shown in the figures: the new UE tune (*red curve*), the new UE tune with the x dependence applied (*blue curve*), the new UE tune with only the scale dependence with $Q_0^2 = 1.0$ GeV^2 applied (*black curve*) and the new UE tune with both x and scale dependence with $Q_0^2 = 1.0$ GeV^2 applied (*pink curve*). The *lower panel* shows the ratio between the various predictions and the predictions obtained with the new UE tune

than 45 GeV while for the second one, $\hat{p}_T$ is required to be greater than 15 GeV. Figure 6 shows the absolute cross sections predicted by the different settings implemented in the PYTHIA 8 simulation.

The red curve shows the predictions for the UE tune with a static value of σ_{eff} while the blue, black, and pink lines represent the predictions obtained when implementing the dynamical x and Q^2 dependence with y equal to 0.5, 1.0, and 2.0 GeV^2, respectively. The highest DPS contribution is observed for $Q_0^2 = 0.5$ GeV^2 and it decreases for increasing Q_0^2 values. The lowest contribution is observed for the static UE tune when no x and Q^2 dependence is applied. The dif-
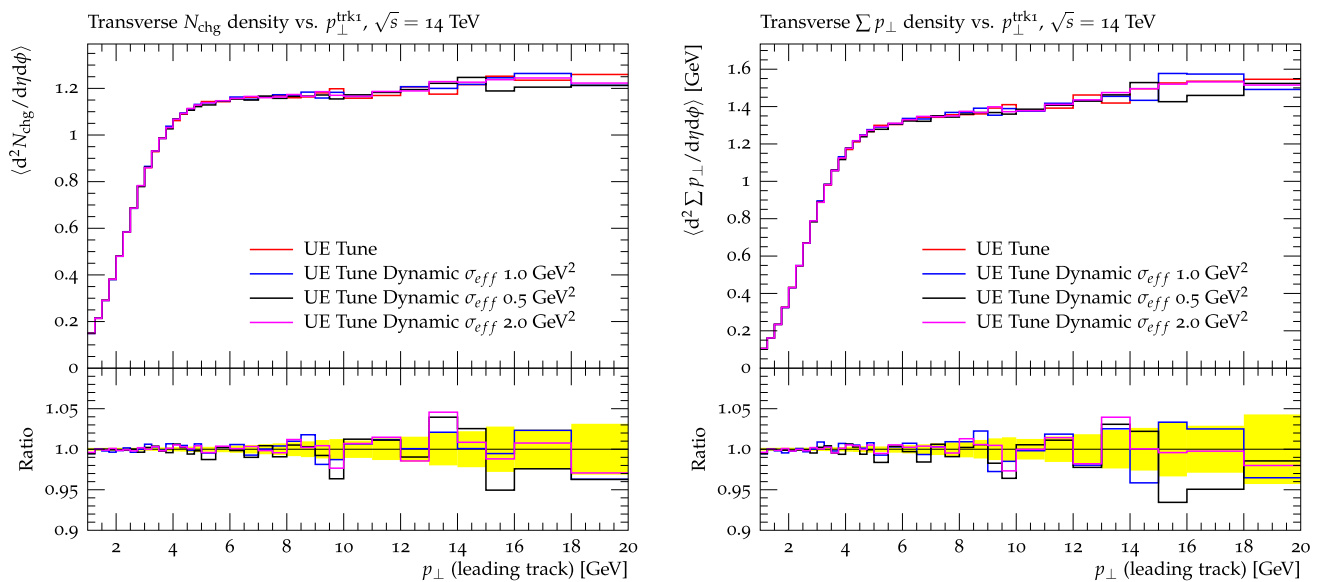
Fig. 7 Charged particle density (*left*) and p_T sum density (*right*) as a function of the leading charged particle in the transverse regions at 14 TeV. Various predictions are shown in the figures: the new UE tune (*red curve*), the new UE tune with both x and scale dependence with difference between the static and the dynamical σ_{eff} tune with $Q_0^2 = 1.0$ GeV^2 (*blue curve*), $Q_0^2 = 0.5$ GeV^2 (*black curve*), and $Q_0^2 = 2.0$ GeV^2 applied (*pink curve*). The *lower panel* shows the ratio between the various prediction and the experimental points

ference between the static and the dynamical σ_{eff} tune with $Q_0^2 = 0.5$ GeV^2 is around 80 %. The different DPS contributions observed among the considered predictions reflect the decreasing σ_{eff} values for decreasing Q_0^2 as a function of the scale of the two scatterings (see the appendix of this paper). No significant differences in the shape of these distributions as a function of Q_0^2 are obtained.

We observed that predictions of a dynamical σ_{eff} tune including a x and scale dependence of the transverse parton distribution are fully consistent with experimental data sensitive to moderate and hard MPI. The good agreement obtained for hard MPI is achieved due to a contribution of the $1 \otimes 2$ mechanism. The contribution from this mechanism is essentially model independent, except for Q_0^2 [25], which is the only new fit parameter, which is expected to lie in the 0.5–2 GeV^2 range.

5 Predictions for 14 TeV

The dynamical σ_{eff} dependence has been tested for predictions of UE and DPS observables at a center-of-mass energy of 14 TeV. The x and scale dependence of σ_{eff} follows, respectively, Eqs. 9 and 10, similarly to the case for 7 TeV. Note that the function R in Eq. 10 also depends on the center-of-mass energy $\sqrt{s}$ [23]. Figure 7 shows predictions of charged particle density and the p_T sum as a function of the leading charged particle p_T, while in Fig. 8 the normalized cross sections as a function of the four-jet correlation observables, ΔS and $\Delta_{\text{soft}}^{\text{rel}} p_T$, are presented. The predictions have been
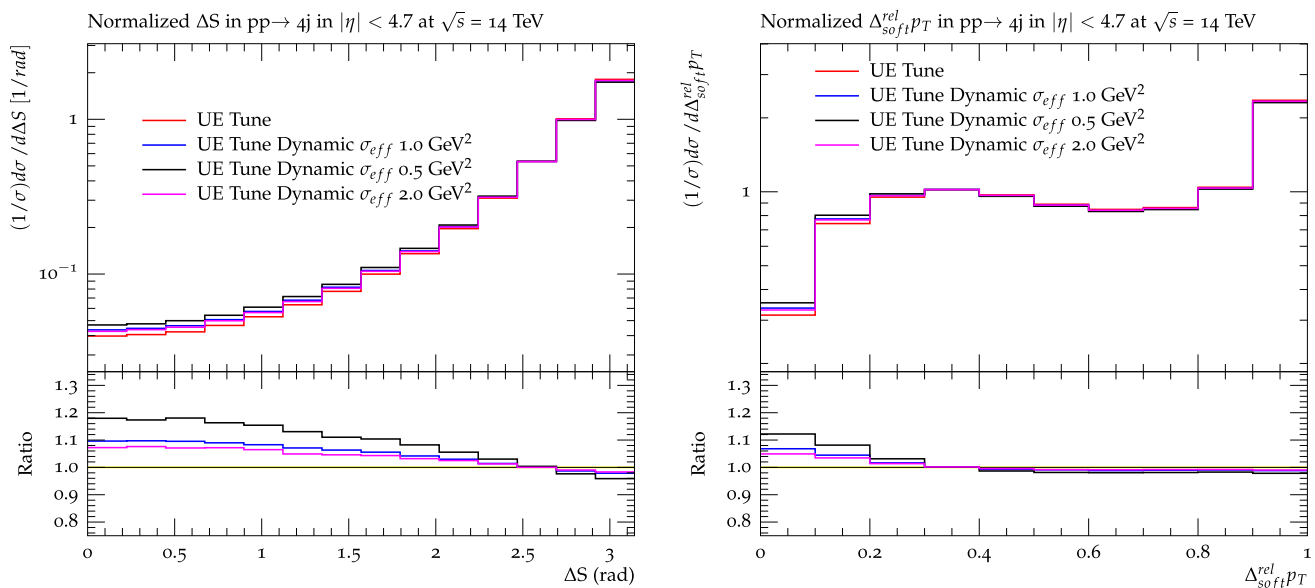
obtained by using the UE tune with a static σ_{eff} value and with a dynamical x- and Q^2-dependent σ_{eff} value, with various values for Q_0^2: 0.5, 1.0, and 2.0 GeV^2.

For each plot, the ratio to the predictions obtained with the UE tune with a constant σ_{eff} value is shown. While for the considered UE observables, a very small change is observed for the various predictions, larger differences are observed when the four-jet correlation observables are investigated. In particular, tunes with a dynamical σ_{eff} dependence tend to predict a higher contribution at low ΔS and $\Delta_{\text{soft}}^{\text{rel}} p_T$ values. These are the regions where a contribution from DPS is expected. The difference between static and dynamical σ_{eff} dependence is of up to 15 % for $\Delta S < 2.0$. Predictions with Q_0^2 equal to 1.0 and 2.0 GeV^2 are very similar to each other, while results obtained with $Q_0^2 = 0.5$ GeV^2 show a higher contribution at low values of ΔS and $\Delta_{\text{soft}}^{\text{rel}} p_T$, where the contribution of hard MPI is expected to be relevant.

6 Comparison with recent Herwig tunes

The calculations described so far in this paper are based on the MPI approach implemented in PYTHIA. A different approach for the description of MPI is implemented in the HERWIG++ event generator [28–31]. Recently, a new tune has been released for the simulation of the UE, labeled UE-EE-5-CTEQ6L1 [30]. This tune is very interesting for the purpose of this paper because it is able to simultaneously describe data sensitive to soft MPI and predict a value of σ_{eff} of about 15 mb, which is much lower than the one in "Pythia

Normalized ΔS in pp→ 4j in $|\eta| < 4.7$ at $\sqrt{s} = 14$ TeV

Normalized $\Delta_{soft}^{rel} p_T$ in pp→ 4j in $|\eta| < 4.7$ at $\sqrt{s} = 14$ TeV

Fig. 8 Normalized cross section distributions as a function of the correlation observables ΔS (*left*) and $\Delta_{\mathrm{soft}}^{\mathrm{rel}} p_T$ (*right*) in a four-jet scenario at 14 TeV. Various predictions are shown in the figures: the new UE tune (*red curve*), the new UE tune with both x and scale dependence with $Q_0^2 = 1.0$ GeV^2 (*blue curve*), $Q_0^2 = 0.5$ GeV^2 (*black curve*), and $Q_0^2 = 2.0$ GeV^2 applied (*pink curve*). The *lower panel* shows the ratio between the various predictions and the predictions obtained with the new UE tune

UE tune". However, the approach of the UE-EE-5-CTEQ6L1 tune is based on a very different picture of both UE and hard MPI from the one discussed in our paper:

- In [28–31], the mean field approximation is used to describe hard MPI, with parameters related to the transverse parton density distribution obtained through a fit to the hard MPI data. The parametrization of the transverse parton distribution corresponds to a dipole form of the two gluon form factor [Eq. (8)] equal to

$$F_{2g} = \left(\frac{1}{1 + \Delta^2/m_g^2} \right)^2 . \tag{13}$$

The parameter μ^2 [28–31] has the same physical interpretation as the parameter m_g^2 introduced in [21,22], measuring the gluonic radius of the proton. In "UE tune Dynamic σ_{eff}" developed in this paper, the transverse parton distributions have been determined from HERA data [19–22], having thus the parameter m_g^2 as a model-independent input. Comparing μ^2 and m_g^2, i.e. comparing the values of the gluonic radii used by tunes UE-EE-5-CTEQ6L1 and "UE tune Dynamic σ_{eff}", respectively, one gets $\mu^2 \sim 2m_g^2$. This means that in the UE-EE-5-CTEQ6L1 tune the gluonic radius of the proton in hard MPI is $\sqrt{2}$ times smaller than the one observed in HERA. In our approach the gluonic radius of the proton is compatible with the one observed at HERA, but in addition to the mean field

approximation, a $1 \otimes 2$ mechanism is included. The contribution of the $1 \otimes 2$ mechanism to hard MPI is of the same order as of the mean field approximation.

- In order to describe UE data and to predict σ_{eff} around 15 mb, the UE-EE-5-CTEQ6L1 tune uses a color reconnecgtion model developed in [31]. In such approach one gets the value of ∼3.9 GeV for the regularization threshold, p_T^0, of the partonic cross section. For "UE tune Dynamic σ_{eff}", the description of UE data and the corresponding parameters are similar to "Pythia UE tune". In particular, the value of p_T^0 implemented in "UE tune Dynamic σ_{eff}" is ∼2.68 GeV (see Table 1).

- The MPI model implemented in HERWIG++ does not lead to any transverse dependence for the value of σ_{eff}, which is taken as a constant as a function of the scale of the secondary hard scattering, in difference from the current approach.

Predictions of the two described HERWIG++ tunes have been compared to data sensitive to hard MPI. Figure 9 shows predictions of the old UE-EE-4-CTEQ6L1 [30] and UE-EE-5-CTEQ6L1 tunes, compared to the normalized distributions as a function of the correlation observables, ΔS and $\Delta_{\mathrm{soft}}^{\mathrm{rel}} p_T$, measured by CMS in four-jet final states at 7 TeV [44]. Predictions from both tunes do not give a good description of the experimental data; the UE-EE-5-CTEQ6L1 tune performs better than UE-EE-4-CTEQ6L1 but differences of around 20–30 % with the data are observed for values of ΔS smaller than 2.5.
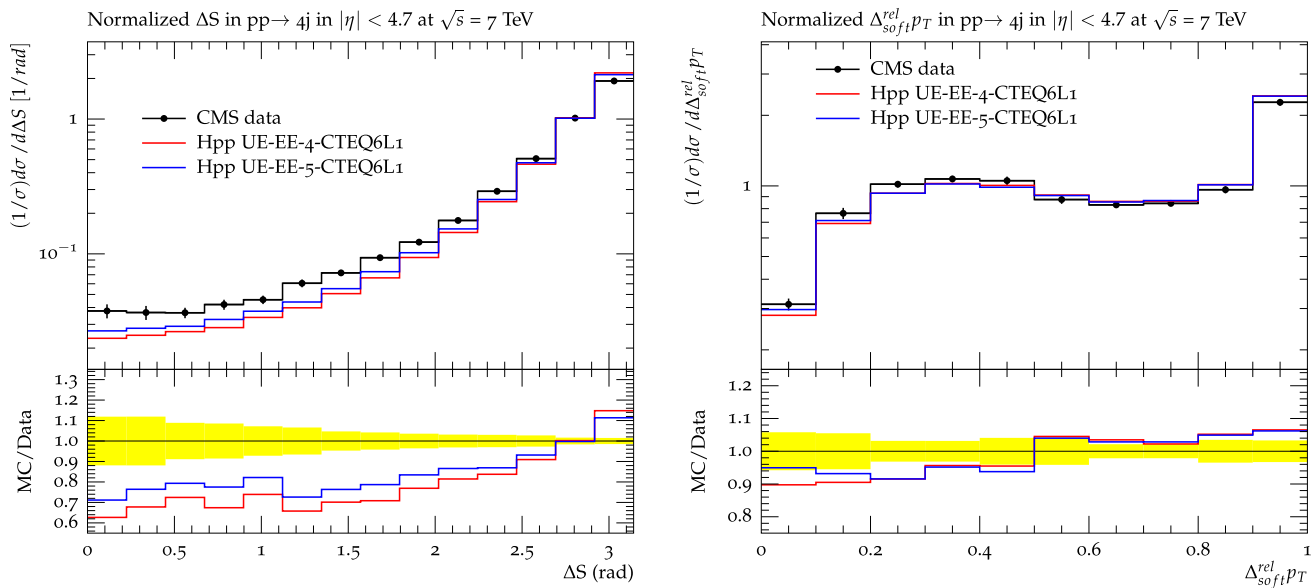
Fig. 9 Normalized cross section distributions as a function of the correlation observables ΔS (*left*) and $\Delta_{soft}^{rel}p_T$ (*right*) measured in a four-jet scenario by the CMS experiment at 7 TeV [44]. The data are compared to predictions obtained with HERWIG ++ tune UE-EE-4-CTEQ6L1 and tune UE-EE-5-CTEQ6L1. The *lower panel* shows the ratio between the various prediction and the experimental points

In conclusion, the approaches used by the "UE tune Dynamic σ_{eff}" developed in this paper and by the HERWIG++ UE-EE-5-CTEQ6L1 tune [30] are rather different and are based on a different picture of both UE and hard MPI. In "UE tune Dynamic σ_{eff}", the emerging treatment of UE is quite close to a mean field approach based on transverse parton densities determined from HERA, and ladder splittings ($1 \otimes 2$ mechanisms) become important in the description of processes with hard MPI. In the approach of the HERWIG++ UE-EE-5-CTEQ6L1 tune, soft and hard MPI are both described in a mean field approach, but with a gluon radius of about 1.4 times smaller than the one obtained from exclusive diffraction measurements at HERA, and a new color reconnection model. No $1 \otimes 2$ mechanism is included. We believe that additional experimental data sensitive to soft and hard MPI will be able in the future to further constrain and eventually discriminate the two approaches.

7 Conclusions

We have developed a new tune "UE tune Dynamic σ_{eff}"[1]. The code modifies the treatment of hard MPI in PYTHIA 8, leading to an improvement in the description of experimental data.

---

[1] The code in RIVET of the two analyses, UE and four-jet measurements, implementing the described event reweighting, can be obtained at the following link: http://desy.de/~gunnep/SigmaEffectiveDependence/.

We do not change the MC code of PYTHIA, but we rather use the results of the MPI simulation on an event-to-event basis, so that $1 \otimes 2$ mechanisms are included.

The tune uses a fit to UE data in order to extract the parameters relative to soft MPI and includes values of σ_{eff}, which contain the $1 \otimes 2$ mechanism. They are calculated directly in the mean field + pQCD approach, as discussed in [25]. The dynamical dependence of σ_{eff} is not derived from a process-dependent fit of the experimental data, but it is directly obtained from theoretical calculations [22–25]. For the parameter Q_0^2, which separates soft and hard scales, we have considered a range of values $0.5 < Q_0^2 < 2$ GeV^2. At present, the accuracy of the experimental data does not allow one to carry through a more precise determination, although the central values of the measured observables are better described by $0.5 < Q_0^2 < 1$ GeV^2. We observe that predictions from such a tune are in good agreement with experimental measurements at 7 TeV, and for the first time they give a consistent description of MPI at both moderate (UE) and hard scales. The results for UE are close to mean field approximation values, as anticipated in [24]. The additional transverse-scale dependence of σ_{eff}, relative to the mean field approach, due to the $1 \otimes 2$ mechanism, is essential for a unified description of UE and hard MPI.

Predictions, obtained with the new tune for proton–proton collisions at 14 TeV, which are expected to happen within the next LHC phase, are also presented.

Appendix A: σ_{eff} dependence at different energies for various scale and longitudinal momentum fraction choices

In this section, a closer look at the σ_{eff} dependence on scale, longitudinal momentum fraction, and collision energy is provided. Figure 10 shows the values of σ_{eff} as a function of the scale of the second interaction for a scale of the first interaction equal to 50 GeV and different choices of Q_0^2 (0.5, 1.0, and 2.0 GeV^2). In this study, the longitudinal momentum fractions of the first interaction system has been set to 0.014, corresponding to the maximal transversality regime. The x value relative to the second hard scattering has also been fixed to the maximal transverse momentum exchange. One can see that σ_{eff} spans over a range of values between 16 and 30 mb, depending on the choice of Q_0^2. The value of σ_{eff} decreases as a function of the scale of the second hard interaction, Q_2, showing a difference of about a factor of 1.1–1.2 between $Q_2 = 15$ GeV and $Q_2 = 40$ GeV. A significant dependence of σ_{eff} on the choice of Q_0^2 is also observed. The smallest σ_{eff} values are obtained for $Q_0^2 = 0.5$ GeV^2,
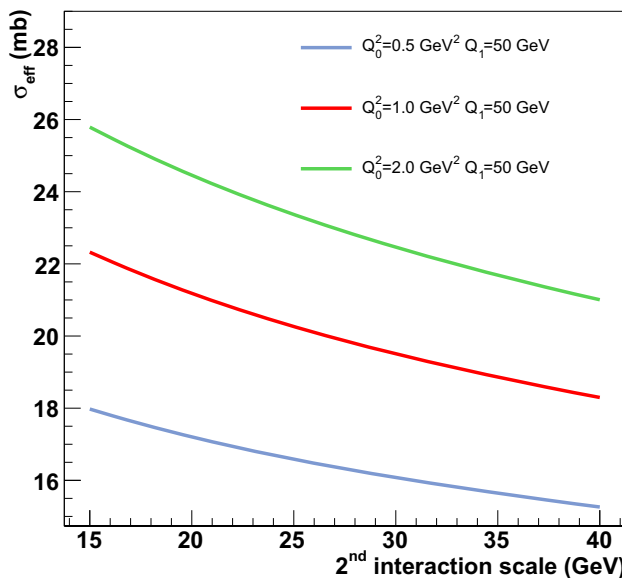
Fig. 10 Values of σ_{eff} as a function of the scale of the second interaction for different scales of the first interaction, Q_1, and different choices of Q_0^2. The values of the longitudinal momentum fractions correspond to the maximal transverse momentum exchange
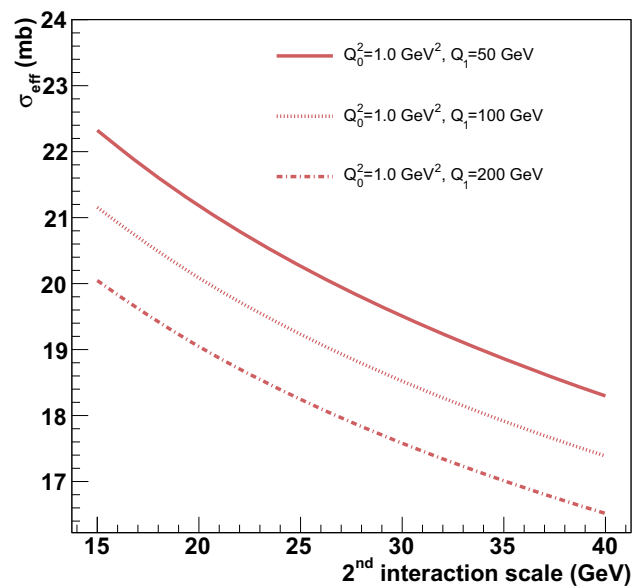
Fig. 11 Values of σ_{eff} as a function of the scale of the second interaction for different scales of the first interaction, Q_1. The value of Q_0^2 has been kept fixed to 1.0 GeV^2
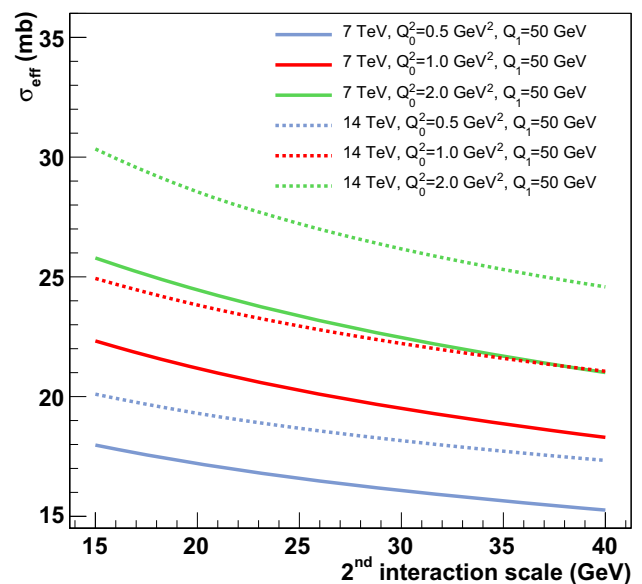
Fig. 12 Values of σ_{eff} as a function of the scale of the second interaction at different collision energies at 7 and 14 TeV for first hard interactions occurring at a scale $Q_1 = 50$ GeV. The three values of Q_0^2 equal to 0.5, 1.0, and 2.0 GeV^2 are considered and the longitudinal momentum fractions of the two dijets correspond to the maximal transverse momentum exchange for both $\sqrt{s} = 7$ TeV and $\sqrt{s} = 14$ TeV

while they increase of roughly a factor of 1.25 and 1.44, for, respectively, $Q_0^2 = 1.0$ and $Q_0^2 = 2.0$ GeV^2.

In Fig. 11, the σ_{eff} dependence is studied for various scales of the first interaction (50, 100, and 200 GeV) corresponding to choices of x_1 and x_2 in the maximum transversality regime, equal to, respectively, 0.014, 0.028, and 0.056. The values of

x_3 and x_4 related to the partons participating in the secondary hard scattering are also set to the maximal exchanged transverse momentum. In this study, only predictions obtained with $Q_0^2 = 1.0$ GeV^2 are shown. It is observed that σ_{eff} does not show a large dependence on the scale of the first interaction: in particular, σ_{eff} decreases as a function of the scale of the first hard scattering. The three curves are very similar between each other as a function of the scale of the second hard interaction and the difference is less than 1 mb.

Figure 12 considers the σ_{eff} variation at different collision energies, 7 and 14 TeV, as a function of the scale of the second hard interaction. The three values of Q_0^2 equal to 0.5, 1.0, and 2.0 GeV^2 are considered. Only scales of the first interaction equal to 50 GeV are examined. The value of σ_{eff} increases for increasing collision energies. For $Q_0^2 = 0.5$ and 1.0 GeV^2, σ_{eff} increases of about 2–3 mb for any scale of the second hard scattering, while for $Q_0^2 = 2.0$ GeV^2, the increase of σ_{eff} is larger and it reaches values of up to 4.5 mb at $Q_2 = 15$ GeV.

References

1. N. Paver, D. Treleani, Nuovo Cim. A **70**, 215 (1982)
2. N. Paver, D. Treleani, Z. Phys. C **28**, 187 (1985)
3. M. Mekhfi, Phys. Rev. D **32**, 2371 (1985)
4. R. Kirschner, Phys. Lett. B **84**, 266 (1979)
5. V.P. Shelest, A.M. Snigirev, G.M. Zinovjev, Phys. Lett. B **113**, 325 (1982)
6. A. Del Fabbro, D. Treleani, Phys. Rev. D **61**, 077502 (2000). arXiv:hep-ph/9911358
7. A. Del Fabbro, D. Treleani, Phys. Rev. D **63**, 057901 (2001). arXiv:hep-ph/0005273
8. A. Accardi, D. Treleani, Phys. Rev. D **63**, 116002 (2001). arXiv:hep-ph/0009234
9. S. Domdey, H.J. Pirner, U.A. Wiedemann, Eur. Phys. J. C **65**, 153 (2010). arXiv:0906.4335 [hep-ph]
10. T.C. Rogers, A.M. Stasto, M.I. Strikman, Phys. Rev. D **77**, 114009 (2008). arXiv:0801.0303 [hep-ph]
11. M. Diehl, PoS D **IS2010**, 223 (2010). arXiv:1007.5477 [hep-ph]
12. M. Diehl, A. Schafer, Phys. Lett. B **698**, 389 (2011). arXiv:1102.3081 [hep-ph]
13. M. Diehl, D. Ostermeier, A. Schafer, JHEP **1203**, 089 (2012). arXiv:1111.0910 [hep-ph]
14. E.L. Berger, C.B. Jackson, G. Shaughnessy, Phys. Rev. D **81**, 014014 (2010). arXiv:0911.5348 [hep-ph]
15. M.G. Ryskin, A.M. Snigirev, Phys. Rev. D **83**, 114047 (2011). arXiv:1103.3495 [hep-ph]
16. J.R. Gaunt, W.J. Stirling, JHEP **1003**, 005 (2010). arXiv:0910.4347 [hep-ph]
17. J.R. Gaunt, C.H. Kom, A. Kulesza, W.J. Stirling, Eur. Phys. J. C **69**, 53 (2010). arXiv:1003.3953 [hep-ph]
18. J.R. Gaunt, W.J. Stirling, JHEP **1106**, 048 (2011). arXiv:1103.1888 [hep-ph]
19. L. Frankfurt, M. Strikman, C. Weiss, Phys. Rev. D **69**, 114010 (2004). arXiv:hep-ph/0311231
20. L. Frankfurt, M. Strikman, C. Weiss, Ann. Rev. Nucl. Part. Sci. **55**, 403 (2005). arXiv:hep-ph/0507286
21. L. Frankfurt, M. Strikman, C. Weiss, Phys. Rev. D **83**, 054012 (2011). arXiv:1009.2559 [hep-ph]
22. B. Blok, Yu. Dokshitzer, L. Frankfurt, M. Strikman, Phys. Rev. D **83**, 071501 (2011). arXiv:1009.2714 [hep-ph]
23. B. Blok, Yu. Dokshitzer, L. Frankfurt, M. Strikman, Eur. Phys. J. C **72**, 1963 (2012). arXiv:1106.5533 [hep-ph]
24. B. Blok, Yu. Dokshitzer, L. Frankfurt, M. Strikman arXiv:1206.5594v1 [hep-ph]. **(Unpublished)**
25. B. Blok, Y. Dokshitzer, L. Frankfurt, M. Strikman, Eur. Phys. J. C **74**, 2926 (2014). arXiv:1306.3763 [hep-ph]
26. J.R. Gaunt, R. Maciula, A. Szczurek, Phys. Rev. D **90**(5), 054017 (2014). arXiv:1407.5821 [hep-ph]
27. J.R. Gaunt, JHEP **1301**, 042 (2013). arXiv:1207.0480 [hep-ph]
28. S. Gieseke, C.A. Rohr, A. Siodmok. arXiv:1110.2675 [hep-ph]. **(Unpublished)**
29. S. Gieseke, D. Grellscheid, K. Hamilton, A. Papaefstathiou, S. Platzer, P. Richardson, C. A. Rohr, P. Ruzicka et al. arXiv:1102.1672 [hep-ph]. **(Unpublished)**
30. M.H. Seymour, A. Siodmok, JHEP **1310**, 113 (2013). arXiv:1307.5015 [hep-ph]
31. S. Gieseke, C. Rohr, A. Siodmok, Eur. Phys. J. C **72**, 2225 (2012). arXiv:1206.0041 [hep-ph]
32. M. Bähr, M. Myska, M.H. Seymour, A. Siodmok, JHEP **1303**, 129 (2013). arXiv:1302.4325 [hep-ph]
33. T. Sjöstrand, S. Mrenna, P.Z. Skands, Comput. Phys. Commun. **178**, 852 (2008). arXiv:0710.3820 [hep-ph]
34. R. Corke, T. Sjöstrand, JHEP **1105**, 009 (2011). arXiv:1101.5953 [hep-ph]
35. R. Corke, T. Sjöstrand, JHEP **1103**, 032 (2011). arXiv:1011.1759 [hep-ph]
36. J.M. Butterworth, J.R. Forshaw, M.H. Seymour, Z. Phys. C **72**, 637 (1996). arXiv:hep-ph/9601371
37. C. Flensburg, G. Gustafson, L. Lonnblad, A. Ster, JHEP **1106**, 066 (2011). arXiv:1103.4320 [hep-ph]
38. F. Abe et al. [CDF Collaboration], Phys. Rev. D **56**, 3811 (1997)
39. V.M. Abazov et al. [D0 Collaboration], Phys. Rev. D **81**, 052012 (2010)
40. V.M. Abazov et al. [D0 Collaboration], Phys. Rev. D **83**, 052008 (2011)
41. G. Aad et al. [ATLAS Collaboration], New J. Phys. **15**, 033038 (2013). arXiv:1301.6872 [hep-ex]
42. S. Chatrchyan et al. [CMS Collaboration], JHEP **1403**, 032 (2014). arXiv:1312.5729 [hep-ex]
43. S. Chatrchyan et al. [CMS Collaboration], JHEP **1312**, 030 (2013). arXiv:1310.7291 [hep-ex]
44. S. Chatrchyan et al. [CMS Collaboration], Phys. Rev. D **89**(9), 092010 (2014). arXiv:1312.6440 [hep-ex]
45. M. Diehl, Phys. Rept. **388**, 41 (2003). arXiv:hep-ph/0307382
46. A.V. Belitsky, A.V. Radyushkin, Phys. Rept. **418**, 1 (2005). arXiv:hep-ph/0504030
47. P. Gunnellini, talk at 6th MPI@LHC symposium, Krakow (2014)
48. B. Andersson, Camb. Monogr. Part. Phys. Nucl. Phys. Cosmol. **7**, 1 (1997)
49. J. Pumplin, D.R. Stump, J. Huston, H.L. Lai, P.M. Nadolsky, W.K. Tung, JHEP **0207**, 012 (2002). arXiv:hep-ph/0201195
50. A. Buckley, J. Butterworth, L. Lonnblad, D. Grellscheid, H. Hoeth, J. Monk, H. Schulz, F. Siegert, Comput. Phys. Commun. **184**, 2803 (2013). arXiv:1003.0694 [hep-ph]
51. A. Buckley, H. Hoeth, H. Lacker, H. Schulz, J.E. von Seggern, Eur. Phys. J. C **65**, 331 (2010). arXiv:0907.2973 [hep-ph]
52. G. Aad et al. [ATLAS Collaboration], Phys. Rev. D **83**, 112001 (2011). arXiv:1012.0791 [hep-ex]